Stress Dependence of Paramagnetic Point Defects in Amorphous Silicon Oxide

Andrea Leto, M. Chiara Munisso, A. Alan Porporati, Wenliang Zhu, and Giuseppe Pezzotti*

Research Institute for Nanoscience, Kyoto Institute for Technology, Sakyo-ku, Matsugasaki, Kyoto 6060-8585, Japan

Received: October 26, 2007; In Final Form: January 21, 2008

Room-temperature red cathodoluminescence (CL) emission (R band) arising from the paramagnetic point-defect population present in amorphous silicon oxide (SiO_x) has been characterized with respect to its shift upon applied stress, according to a piezo-spectroscopic (PS) approach. The R band (found at around 630 nm) originates from nonbridging oxygen hole centers (NBOHC; $\equiv Si-O^\bullet$) generated in the presence of oxygen-excess sites. It is shown that reliable stress assessments can be obtained in silica glass with a relatively high spatial resolution, provided that appropriate spectroscopic procedures are developed to precisely extract from the CL spectrum the shift upon stress of the R band, isolated from other partly overlapping bands. Macroscopic and microscopic PS calibration procedures are shown to lead to consistent results on silica materials with different chemical characteristics and, thus, with different intrinsic defect populations. In addition, quantitative calibrations of both electron probe size and luminescence emission distribution within the electron probe are given. As an application of the PS technique, the magnitude of the residual stress piled up (mainly due to a thermal expansion mismatch) at a sharp silica/silicon interface has been characterized by taking into account the gradient in defect population developed as a function of distance from the interface. In the Results and Discussion section, brief comments are offered regarding the possible impact of highly spatially resolved stress assessments in silica glass upon the development of new materials and advanced electronic devices.

1. Introduction

Luminescence spectra arising from lattice defects (i.e., interstitial/substitutional ions and vacancies) have been often used in the characterization of chemical structure in amorphous materials.[1−3] The basic idea behind this spectroscopic approach has been that the luminescence properties of selected defects may reflect not only the structural state of the defect itself but also that of its chemical surroundings in the host structure. From this perspective, luminescence spectra from native impurities or intentionally added luminescent ions have been used in chemical and crystallization analyses of amorphous materials.[4,5] Concurrently, efforts have been made toward the quantitative characterization of point-defect population in silica glass, given the importance of this material as a dielectric gate component in semiconductor technology.[6] In both cases, luminescence spectroscopy yielded structural information of a completely different character from that obtainable by diffraction-based techniques, the latter detecting long-range order while the former yielded information on the immediate surroundings of a luminescent ion (thus, being particularly useful as a structural probe in short-range amorphous structures).

Owing to the unique ability of defect luminescence in bringing local information about the host matrix, we have recently proposed its use as a highly localized stress (or strain) sensor within either glassy or crystalline structures.[7−9] The physical principle behind the stress assessment resides in the piezo-spectroscopic (PS) effect, namely, the spectral shift observed for selected luminescence bands emitted from a stressed atomic structure as compared to an unstressed (reference) state. When excited with a focused electron probe, the (cathodo)luminescence (CL) emission can be confined to a very localized area (i.e., on the sub-micrometer scale), and this represents a main

advantage in stress assessments, especially in highly graded stress distribution. Another tangible advantage in using point defects as a stress probe is that, although the defect represents itself a local perturbation of the host structure, the "image" stress felt by the CL probe can be easily transformed into the actual stress field in the surrounding host matrix by means of suitable PS calibration procedures.[7−9]

In this paper, we discuss the feasibility of using the CL activity of the paramagnetic defects present in an amorphous silica glass network as a sensor in highly spatially resolved stress assessments. The CL emission from silica glass is first revisited in both its physical and spectroscopic meanings. Then, PS and probe calibration data are shown for amorphous silicon oxides (SiO_x) with different chemical structures as paradigm glass materials. The understanding obtained from this basic analysis provides the foundation for applications of the CL/PS technique to the determination of the residual stress fields stored in actual devices after processing, use, and manipulation (e.g., Si/SiO_2 semiconductor devices). Applied aspects of CL/PS stress microscopy in actual electronic devices have been discussed in detail elsewhere.[10]

2. Experimental, Calibration, and Computational Procedures

A. Materials and Equipment. The high-purity silicon oxide material investigated was a specially manufactured strain-free silica glass (ES Grade, Tosoh Co., Tokyo, Japan). Nonstoichiometric carbon-doped SiO_x (simply referred to as C-doped SiO_x, henceforth) was obtained from a large pool of the interlayer dielectric material comprised in a Cu/Ta-interconnect metal-oxide−silicon pattern belonging to a model electronic chip (Intel Corp., Santa Clara, CA). The SiO_x/Si interface studied as an application of the PS technique belonged to an intermediate unit of a metal-oxide semiconductor (MOS) chip prepared by chemical vapor deposition (CVD).

* To whom correspondence should be addressed. E-mail: pezzotti@kit.ac.jp.
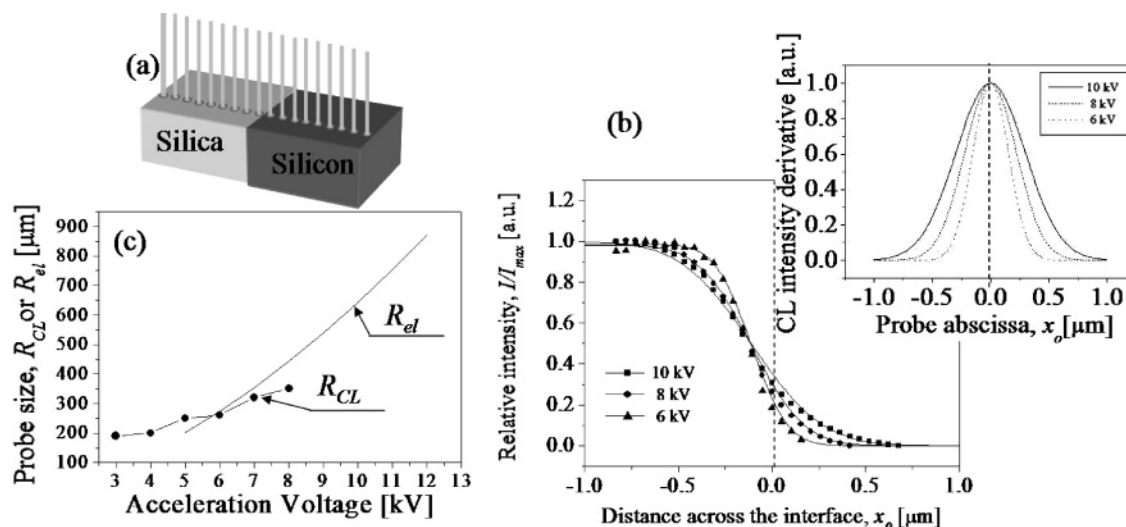
Figure 1. (a) Schematic of a line scans across a sharp and straight interface between the SiO_x material and silicon; (b) the probe response function, PRF, of the material, as a function of acceleration voltage, obtained from the first derivative of the normalized intensity functions; (c) a plot of cathodoluminescence, CL, probe size as a function of acceleration voltage, $R_{CL}(V)$, compared with a plot of electron probe size $R_{el}(V)$.

A field-emission gun scanning electron microscope (FEG-SEM) was used as the excitation source for CL emission throughout this work. This was a Schottky-emission-type gun (HITACHI S-4300SE, Hitachi, Tokyo, Japan). The FE-SEM device was mounted on an air-suspended optical table in order to minimize the effect of vibrations in high-resolution measurements and to aid optical alignment. A high-sensitivity CL detector unit (MP-32FE, Horiba Ltd., Kyoto, Japan) was attached to both microscopes for the collection of light upon reflection into an ellipsoidal mirror and transmission through an optical fiber. The emitted light spectrum was analyzed using a single monochromator (TRIAX 320, Horiba-Jobin Ivon-Spex) equipped with a CCD camera. A triple-grating spectrograph was equipped with one ruled grating (150 gr/mm) and two blazed holographic gratings (1200 and 1800 gr/mm), which were mounted on a rotating triple-grating turret. A mapping device (PMT R943-02 Select, Horiba Ltd., Kyoto, Japan) and related software enabled us to collect maps with improved spatial resolution and to perform automatic analysis of a large number of spectra. The signal from a neon discharge lamp was collected concurrently to the CL spectra for obtaining an independent spectral calibration of the spectrometer. A 2 nm thick layer of platinum was deposited on the samples to avoid charging induced by electron beam irradiation.

B. Assessments of Luminescence and Electron Probe Sizes. In spatially resolved CL spectroscopic assessments, the selection of a low acceleration voltage helps to minimize probe size and intrusiveness; however, the statistical reliability of the obtained CL spectrum may dictate a lower limit for the selected probe size. In particular, a statistically reliable spectrum of suitable intensity can only be achieved by using acceleration voltages higher than a given critical value, which depends on the luminescence emission efficiency of the studied material. Furthermore, it should be noted that the shallow nature of the electron probe may lead to CL emission being effected by surface effects (e.g., surface plasmons and roughness).[11] Therefore, in selecting the acceleration voltage, a compromise is usually required between spatial resolution and statistical reliability of collected spectra. Given the importance of the probe issue in PS assessment, a detailed knowledge of probe size and morphology is required.[12] Such a knowledge may help to counteract the spatial resolution problems arising from a finite probe size. As a first step in the assessment of the CL probe, a probe response function (PRF) can be experimentally retrieved as a function of acceleration voltage from line scans across a sharp and straight interface between the SiO_x material and silicon (Figure 1a). This procedure, which has been shown in detail in previous papers,[13,14] consists of obtaining the first derivative of an experimental plot of the relative CL intensity as a function of distance between the geometrical center of the electron probe and the interface. In the absence of crystallographic textures and anisotropy (which applies to an SiO_x amorphous material), the derivative plot obeys, to a degree of precision, a Gaussian function (i.e., the PRF $G(x,x_0,V)$), as follows

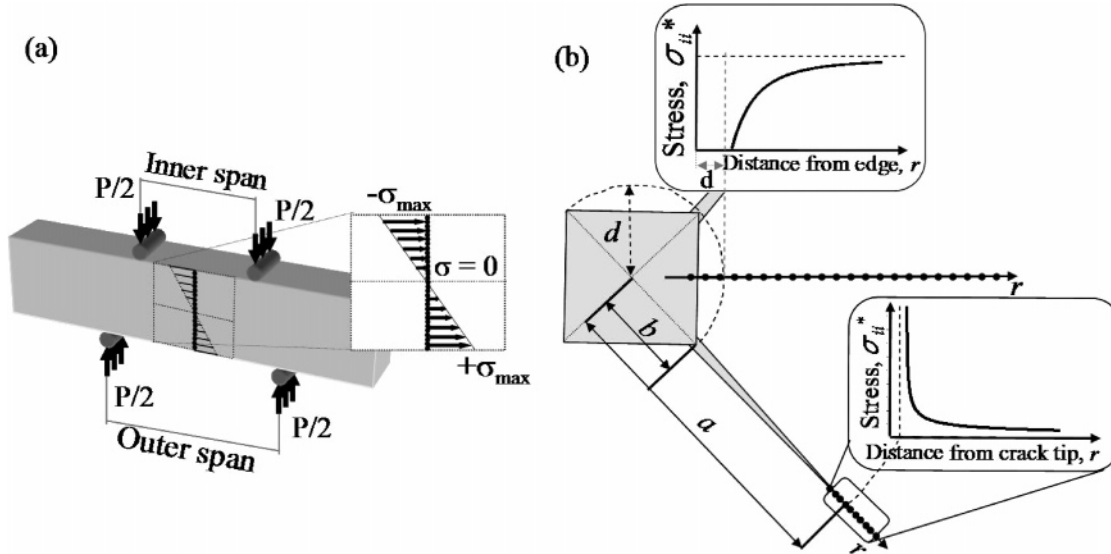$$G(x,x_0,V) = C_1 \exp \frac{-(x - x_0)^2}{C_2 V^n} \tag{1}$$

where the parameter V is the acceleration voltage, and the abscissas, x and x_0, represent a general point in the focal plane and the geometrical center of the focused electron beam, respectively. The parameter, C_1, can be taken equal to unity after intensity normalization. In first approximation, the CL probe can be considered symmetric in the measurement plane, and its size, R_{CL}, is defined according to the following equation

$$\frac{\int_{x_0-R_{CL}}^{x_0+R_{CL}} G(x,x_0,V)dx}{\int_{-\infty}^{+\infty} G(x,x_0,V)dx} = 0.9 \tag{2}$$

where the factor 0.9 is an arbitrarily selected threshold value for CL intensity contributions from remote parts of the electron probe. The CL probe size may differ from the primary electron probe range, R_{el}, which is also a function of acceleration voltage, V. The electron probe size can be calculated according to the Kanaya−Okayama equation[15]

$$2R_{el} = \frac{2.76 \times 10^{-2} \times A}{\rho Z^{0.889}} V^{1.67} \tag{3}$$

where ρ is the material density, A its atomic mass number, and Z its atomic number (e.g., 2.2 g/cm^3, 60 g/mol, and 30, respectively, for silica glass).

Stress Dependence of Paramagnetic Point Defects

J. Phys. Chem. A, Vol. 112, No. 17, 2008 **3929**

Figure 2. Schematic drafts describing the three methods of PS calibration. (a) The four-point bending flexure method; (b) the indentation crack-tip method and the indentation print-edge method.

The differential contribution from each portion of volume in the luminescent probe (i.e., the PRF of the material), as obtained from the first derivative of the normalized intensity functions, is shown in Figure 1b as a function of acceleration voltage. The best fit to the experimental data collected at different voltages, as obtained according to eq 1, was achieved when the probe-related parameters C_2 and n were selected as 0.022 and 1.05, respectively. A plot of probe size as a function of acceleration voltage, $R_{CL}(V)$, was then obtained according to eq 2. This plot is given in Figure 1c and compared with a plot of electron probe size, as obtained according to eq 3. Plots of probe size revealed that at voltages $V < 5$ kV, the R_{CL} was systematically larger than R_{el}, suggesting that internal light diffusion plays a role in the highly transparent silica material. On the other hand, for $V > 5$ kV, R_{CL} was lower than R_{el}, most likely due to internal absorption. Despite probe broadening, these plots demonstrate that the size of the CL probe in silica glass can be confined into a sub-micrometer order. The policy followed in the present CL measurements of silica glass was that of selecting a relatively high acceleration voltage ($V = 8$ kV), thus partly sacrificing probe sharpness, in order to obtain a clear and stable CL spectrum.

C. Macroscopic and Microscopic PS Calibrations. The PS behavior of a given electronic transition is characterized by the wavelength shift, $\Delta\lambda$, with respect to a reference unstressed state which the CL band representative of the transition obeys when an elastic stress field is applied. The stress state is represented by a second-rank tensor, σ_{ij}, which is related to the scalar quantity, $\Delta\lambda$, by a tensorial equation, as proposed by Grabner[16]

$$\Delta\lambda = \Pi_{ij}\sigma_{ij} = \Pi_{ii}\sigma_{ii}^* = \Pi(\sigma_{xx}^* + \sigma_{yy}^* + \sigma_{zz}^*) \qquad (4)$$

where $i,j = x,y,z$; $\Delta\lambda = \lambda - \lambda_0$ is the wavelength shift observed for the material under stress with respect to a reference "stress-free" wavelength, λ_0; Π_{ij} is the second-rank tensor of PS coefficients, and the repetitive index notation applies to eq 4. However, it should be noted that in a glassy material, the PS tensor degenerates into a scalar quantity, usually referred to as the PS coefficient, Π. In other words, according to eq 4, $\Delta\lambda$ is an invariant with respect to the choice of a system of Cartesian coordinates, and thus, it directly relates to the scalar summation of the principal stress components or, in other words, to the trace of the stress tensor. The Π value depends both on the

investigated material and on the spectroscopic band selected in the CL spectrum and should be retrieved according to preliminary calibrations. Note that we again come across a limitation in reducing probe size, which is that the PS measurement should be averaged over a (statistically meaningful) large number of defect clusters, optically activated by the electron probe.

Three methods of PS calibration were employed for generating known stress fields into the silica materials investigated: (i) the four-point bending flexure method; (ii) the indentation crack-tip method; and, (iii) the indentation print-edge method. Schematic drafts describing the above three methods are given in Figure 2a and b.
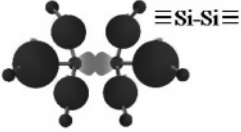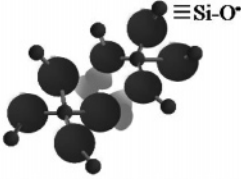
In the four-point bending method, a flexural microjig, equipped with a load cell of 100 N, is placed into the electron microscope. After loading the bending bar, CL spectra are mapped along the bar thickness (cf. Figure 2a). During the time necessary for collecting luminescence spectra in the above materials, care should be taken that no significant relaxation occurs in the loading jig. In this calibration method, the obtained stress field is of an uniaxial nature and involves both compressive and tensile stress magnitudes (indicated with a positive and negative sign, respectively), whose maxima are found in correspondence of the surfaces in contact with the short- and the long-span loading bars of the jig, respectively. The stress field is linear along the specimen thickness and constant along the specimen depth. As far as a linear stress field is involved, the longitudinal axis at the center of the bar thickness (i.e., the neutral axis) should be stress-free. The PS equation can be written in terms of the principle stress tensor and the PS eq 4 simply rewritten as follows

$$\Delta\lambda = \Pi\sigma_{ii}^* = \Pi\begin{bmatrix} \sigma_{xx} & 0 & 0 \\ 0 & 0 & 0 \\ 0 & 0 & 0 \end{bmatrix} = \Pi\sigma_{xx}(y) \qquad (5)$$

where the stress field, $\sigma_{xx}(y)$, is uniaxial and involves both compressive and tensile stresses, calculated from the applied load, P, according to the following equation

$$\pm\sigma_{max} = \pm\frac{3P(L-l)}{2wh^2} \qquad (6)$$

TABLE 1: Summary of the Salient CL Features Reported for Optically Active Defects in Amorphous Silica Structures

Defect type	Symbol	Energy level [eV]	Maximum band [nm]
Oxygen Deficiency Centers (ODC)	$\equiv$Si–Si$\equiv$	2.7	460 (*B*)
Non-Bridging Oxygen Hole Centers (NBOHC)	$\equiv$Si–O$^{\bullet}$	1.9	650 (*R*)
UV Band	$\equiv$Si$^{\bullet}$	4.3	290 (*UV*)
Contamination band	—	2.3–2.2	530–550 (*Y*)

where L and l are the long and the short spans, respectively, and w and h are the sample width and thickness, respectively.

A Vickers indentation generates a tens of μm sized squared print on the material surface with stably propagated microcracks extending from each of the four corners of the print. The stress field developed along a straight line ahead of an indentation microcrack is of a biaxial (tensile) nature and can be precisely assessed, provided that an additional measurement of crack-opening displacement (COD) is made in the FEG-SEM.[17] In addition, also the residual stress field generated along a straight line perpendicular to the edges of the indentation print (cf. Figure 2b) can be rationalized in terms of known parameters[18,19] and used for PS calibration. Note that the latter two microscopic calibration methods were selected in this study because no bulk specimen of relatively large size (e.g., suitable for macroscopic four-point bending loading) was available for the C-doped SiO$_x$ material. In the crack-tip PS calibration method, after converting the biaxial stress components into principle stress components and neglecting higher-order terms, the Grabner's eq 4 can be rewritten at any location ahead of the crack tip as follows[20]

$$\Delta\lambda = \Pi\sigma_{ii}^* =$$

$$\Pi\frac{K_{\mathrm{I}}}{\sqrt{2\pi r}}\cos\frac{\theta}{2}\begin{bmatrix} 1+\sin\dfrac{\theta}{2} & 0 & 0 \\ 0 & 1-\sin\dfrac{\theta}{2} & 0 \\ 0 & 0 & 0 \end{bmatrix} = \frac{2\Pi K_{\mathrm{I}}}{\sqrt{2\pi r}}\cos\frac{\theta}{2} \quad (7)$$

where K_{I} is the crack-tip stress intensity factor ($K_{\mathrm{I}} = 0.83$ MPa·m$^{1/2}$ for C-doped SiO$_x$) and r and θ are polar coordinates, as depicted in Figure 2b.

In the print-edge PS calibration method, the Grabner's eq 4 can be rewritten at any location on the surface of the material along a line perpendicular to the edge of the indentation print (cf. Figure 2b) as follows

$$\Delta\lambda = \Pi\sigma_{ii}^* =$$

$$-\Pi\frac{4B}{r^3}\begin{bmatrix}(2-\nu) & 0 & 0 \\ 0 & 0 & 0 \\ 0 & 0 & (2\nu-1)\end{bmatrix} = -\Pi\frac{4B}{r^3}(1+\nu) \quad (8)$$

where ν is the Poisson's ratio of the silica material ($\nu = 0.17$) and the constant B is given by

$$B = \frac{\dfrac{E}{2(1+\nu)}d^3\tan\beta}{2(1-2\nu)} \quad (9)$$

with E being the Young's modulus of the silica material ($\approx$78 GPa), β the geometrical angle of the indenter, and d the radius of the plastic zone ($d \approx 32$ μm for an indentation load of $P = 5$ N).

It should be noted that, unlike the case of the linear stress field in the macroscopic configuration of a bending bar, in the described microscopic stress fields, the stress gradients can be quite steep, and consequently, the observed wavelength shift (with respect to an unstressed location) represents a spatial convolution of the local stress distribution. For the crack-tip stress field, the convoluted band shift is related to the stress tensor trace by

$$\overline{\Delta\lambda}(x_0,y_0;V) = \frac{\int_{-\infty}^{+\infty}\int_{-\infty}^{+\infty}G(x,x_0,y,y_0;V)\times\Delta\lambda(x,y)\mathrm{d}x\mathrm{d}y}{\int_{-\infty}^{+\infty}\int_{-\infty}^{+\infty}G(x,x_0,y,y_0;V)\mathrm{d}x\mathrm{d}y}$$

$$= 2\Pi K_{\mathrm{I}}\frac{\displaystyle\int_0^{+\infty}\int_{-\pi}^{+\pi}\frac{r}{\sqrt{2\pi r}}\cos\frac{\theta}{2}\times\exp\left(-\frac{r^2+x_0^2}{C_2V^n}\right)\times\exp\left(\frac{2rx_0\cos\theta}{C_2V^n}\right)\mathrm{d}r\mathrm{d}\theta}{\displaystyle\int_0^{+\infty}\int_{-\pi}^{+\pi}r\exp\left(-\frac{r^2+x_0^2-2rx_0\cos\theta}{C_2V^n}\right)\mathrm{d}r\mathrm{d}\theta}$$

$$= \Pi\overline{\sigma}_{ii}^*(x_0,0,0) \quad (10)$$

Stress Dependence of Paramagnetic Point Defects

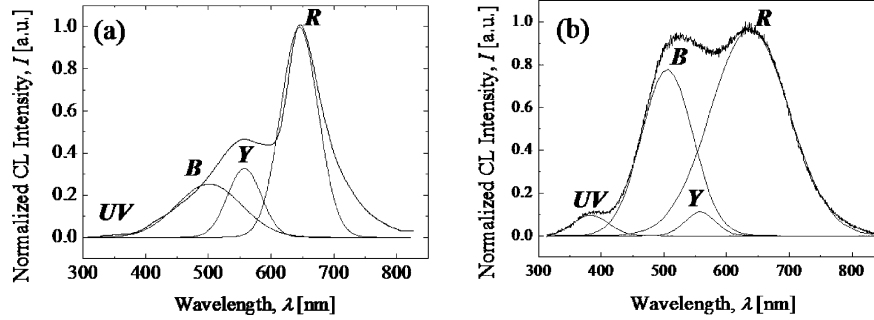*J. Phys. Chem. A, Vol. 112, No. 17, 2008* **3931**

Figure 3. Typical CL spectra collected in a highly pure silica (a) and a C-rich silica glass (b).
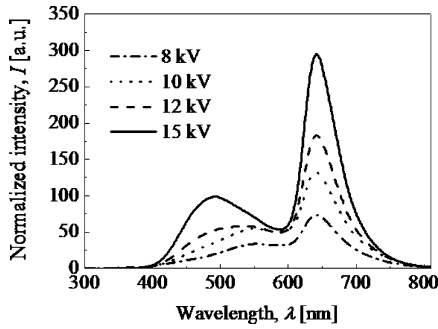

Figure 4. The evolution of the CL spectrum of pure silica, as recorded upon changing the electron acceleration voltage (at constant beam power).

where $\bar{\sigma}_{ii}^{*}(x_0,0,0)$ is the convoluted (equi-biaxial) stress value at any location $P \equiv (x_0,0,0)$ straight ahead of the crack tip. The PRF, $G(x,x_0,V)$, is the Gaussian curve corresponding to the selected acceleration voltage, as shown in Figure 1b. According to a similar approach, in the case of the print-edge stress field, the wavelength shift (with respect to an unstressed location) collected in the probe volume represents a convolution of the surface stress field and can be expressed by

$$\overline{\Delta\lambda}\left(r_0,\frac{\pi}{2},0,V\right) = \frac{\int_{-\infty}^{+\infty}\int_{-\pi}^{+\pi} G(r,r_0;V)\times\Delta\lambda(r,\theta)\mathrm{d}r\mathrm{d}\theta}{\int_{-\infty}^{+\infty}\int_{-\pi}^{+\pi} G(r,r_0;V)\mathrm{d}r\mathrm{d}\theta}$$

$$= 4\Pi B(1+\nu)\times$$

$$\frac{\int_{0}^{+\infty}\int_{-\pi}^{+\pi}\frac{1}{r^2}\times\exp\left(-\frac{r^2+r_0^2}{C_2 V^n}\right)\times\exp\left(\frac{2rr_0\cos\theta}{C_2 V^n}\right)\mathrm{d}r\mathrm{d}\theta}{\int_{0}^{+\infty}\int_{-\pi}^{+\pi} r\exp\left(-\frac{r^2+r_0^2-2rr_0\cos\theta}{C_2 V^n}\right)\mathrm{d}r\mathrm{d}\theta}$$

$$= \Pi\bar{\sigma}_{ii}^{*}\left(r_0,\frac{\pi}{2},0\right) \qquad (11)$$

where $\bar{\sigma}_{ii}^{*}(r_0,\pi/2,0)$ is the convoluted trace stress tensor at any location $P \equiv (r_0,\pi/2,0)$ along a radius perpendicular to the print edge and with its center at the geometrical center of the indentation print. More details about the stress convolution procedure in microscopic PS calibrations have been given elsewhere.[20] Equations 5, 10, and 11, which can be numerically solved for Π with the aid of commercially available computing software,[21] constitute the foundation for experimentally calibrating the PS behavior of CL bands selected among those emitted by optically active defects in amorphous silica.

3. Results and Discussion

A. Optically Active Point Defects in Silica Glass. The CL spectrum of silica glass mainly consists of three partly overlap-

ping bands: (i) one band in the blue region at about 460 nm (referred to as band B, henceforth) arising from oxygen-deficiency-related centers (ODC) or twofold-coordinated silicon centers ($\equiv$Si$-$Si$\equiv$), which are generated in the presence of oxygen vacancy sites;[6] (ii) one band in the red region at around 630 nm (R band), which is related to nonbridging oxygen hole centers (NBOHC; $\equiv$Si$-$O$^\bullet$) and generated in the presence of oxygen-excess sites;[6] and (iii) one ultraviolet band at about 290 nm (UV band) whose origin has been attributed to trivalent silicon centers ($\equiv$Si$^\bullet$) and other point defects generated by electron beam irradiation.[6] Additional bands arising from impurities have also been reported;[16] in particular, the presence of amorphous carbon, either introduced during processing of the glass or arising from electron beam contamination, produces a relatively intense and broad band located at around 415 nm[6] (the yellow band, Y), thus partly overlapping both the B and R bands. A typical feature of C-rich silica is the limited intensity of the R band, as a consequence of the partial elimination of oxygen-excess centers.[19] The oxygen-vacancy-related B band has recently been reported to actually consist of two distinct sub-bands of similar intensity, located at 445 and 480 nm. However, both bands arise from polymorphism of the same kind of defect (i.e., the ODC: $\equiv$Si$-$Si$\equiv$).[22] A summary of the salient CL features reported for optically active defects in amorphous silica structures is given in Table 1. Typical CL spectra collected in a highly pure and a C-rich silica glass are shown in Figure 3a and b, respectively. A spectral deconvolution into four Gaussian sub-bands is also given for both spectra, according to a semiquantitative fitting procedure involving the three main defect bands and the C-related band, as reported in the literature (cf. Table 1). In Figure 3, both spectra were collected under the same electron irradiation conditions (i.e., 8 kV, 73 pA, 10 s) and normalized with respect to their respective maxima. Three main features can be noticed in comparing the CL spectra retrieved from silica materials with different chemical characteristics: (i) the R band is clearly preponderant on the B band in the C-free sample, while the R and B intensities are comparable in pure silica; (ii) the UV band is relatively intense in C-rich silica (i.e., intensity comparable with the Y band), while it is negligibly small in pure silica as compared to the two main bands; and, (iii) in both spectra, the Y band partly overlaps both the R and B bands and disturbs spectral symmetry, thus rendering the spectral deconvolution ill-defined. This latter circumstance greatly complicates the PS analysis, as shown in a forthcoming section, and calls for alternative procedures with respect to sub-band deconvolution for correctly extracting the magnitude of PS shifts of selected CL sub-bands.
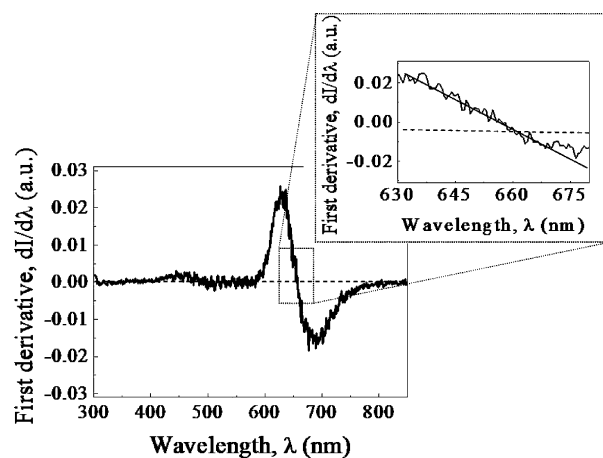
B. Spectroscopic Analysis of CL Emission in Silica Glass. The evolution of the CL spectrum of pure silica, as recorded upon changing the electron acceleration voltage (at constant beam power), is shown in Figure 4. The most striking feature
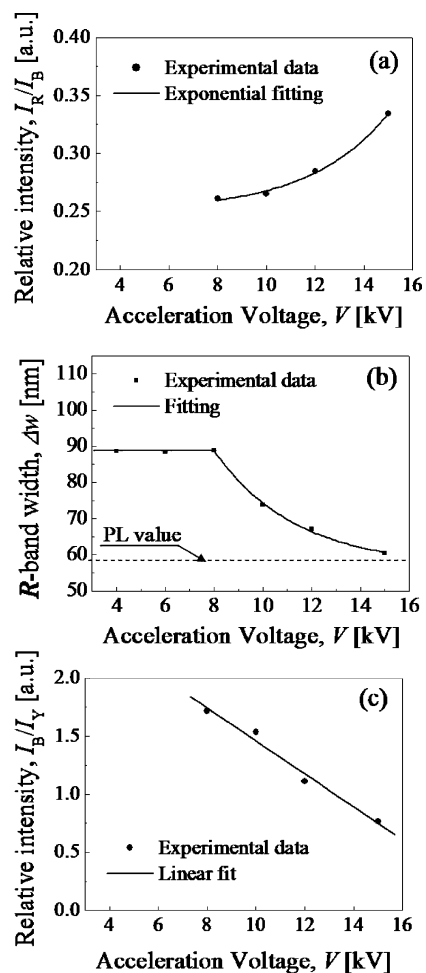
Figure 5. (a) Plot of the relative intensity of the R band over the B band, (b) R-band fwhm, and (c) relative intensity of the B band over the Y band, as a function of the acceleration voltage.

Figure 6. The R-band maximum was retrieved by performing a first derivative of the smoothed spectrum with respect to wavelength and then finding the intercept of the derivative curve with the wavelength abscissa.


Figure 7. The dependence on the stress of the spectral position of the oxygen-excess R band located at around 630 nm, when excited at 8 kV. The plot is cumulative for the two materials investigated and for the three types of calibration methods (i.e., four-point bending and indentation crack-tip and print-edge calibrations).

in the plot is that the ratio of intensities of the labeled bands is not constant with changing electron irradiation conditions. In other words, the defect population excited by the probe in the material varies with varying irradiation energy. In particular, the relative intensity of the R band significantly increases and its full-width at half-maximum (fwhm) decreases with increasing acceleration voltage. In addition, the two main maxima of the CL spectrum, namely, the peak top of B and R, tend to separate from each other with increasing irradiation energy. As a minor feature, the intensity of the UV band decreases with increasing of the selected acceleration voltage. Figure 5a, b, and c shows plots of relative intensity of the R band over that of the B band (band maxima are assumed in first approximation to equal the two main observed maxima of the overall CL spectrum), the R-band fwhm, and relative intensity of the B band over that of the Y band as a function of acceleration voltage, respectively. In the inspected voltage interval, the relative intensity of the R band was found to increase with voltage according to a nonlinear trend (cf. Figure 5a). No saturated state could be observed. On the other hand, the fwhm of the R band typically remained constant up to $V \approx 8$ kV, to successively decrease according to an exponential trend at higher voltages. Interestingly, the bandwidth decrease appears to saturate at around 60 nm (cf. Figure 5b), a value which was reported for the width of the R band in ultraviolet laser photostimulated spectra.[23] In order to visualize the spectral changes described above, one may imagine that, phenomenologically speaking, the CL spectrum of pure SiO_x "unfolds" with increasing excitation energy, with the R
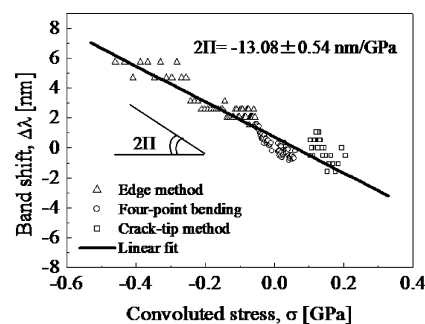
band being more pronounced and, more importantly, becoming increasingly isolated from the rest of the spectrum. Unfortunately, unlike the pure silica material, the CL spectrum of C-doped silica was conspicuously invariant with respect to the selected electron irradiation condition.

The presence of hydrogen has been proposed to be one of the causes for the formation of the R band.[22] Upon irradiation, H^+ diffuses away, and NBOHC are formed, resulting in an increase of the red-band emission until diffusion of the available H^+ ends off. Defects related to structural water have also been assumed as possible precursor centers. Koyama[24] assumed that emission may originate from hydrogen in the form of OH^- or adsorbed H_2O in the quartz lattice. The CL spectral variations observed in the present materials are in line with results as a function of electron irradiation conditions previously published by Koyama[24] for silica glasses prepared according to different procedures. CL bands from optically active defects in silica appear to vividly represent the structural features of the amorphous network. Besides these structural features, we shall show in the next sections that, under suitable electron irradiation conditions, the CL spectrum can be also used to probe local stress states stored in the amorphous SiO_x network.

C. PS Behavior of the R Band of Silica Glass. A fundamental step in developing a reliable PS stress assessments method in amorphous silica is to establish a spectroscopic procedure capable of precisely extracting band shift from the recorded CL spectra. Sharp luminescence bands (e.g., those arising from rare-earth impurities) are usually fitted to Gaussian, Lorentzian, or to their mixed functions.[9] However, given the

Stress Dependence of Paramagnetic Point Defects

J. Phys. Chem. A, Vol. 112, No. 17, 2008 **3933**
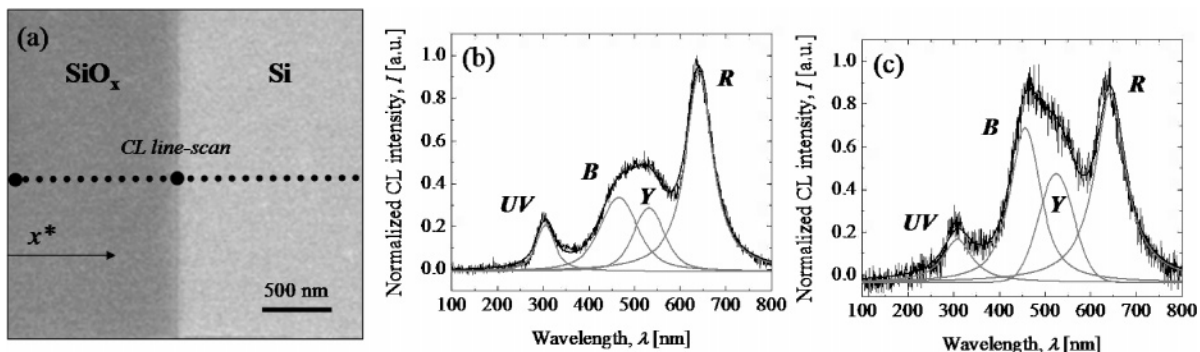
Figure 8. (a) A FEG-SEM micrograph taken at the SiO_2/Si interface of an intermediate unit in a CVD MOS device. Several line scans were collected at different acceleration voltages (6, 8, and 10 kV) along a selected line x^*. (b) Two typical CL spectra collected at a location far away from the interface and (c) exactly centered at the SiO_x/Si interface.

conspicuous spectral overlapping found in the CL emission from different families of defects in amorphous silica, no reliable deconvolution/fitting algorithm for the retrieved CL spectra could be found in this study. To tackle this problem, methods for extracting band shift information from the CL spectra with improved precision were attempted as follows. On the basis of the spectroscopic analysis performed on the pure silica material, we selected an acceleration voltage of $V = 8$ kV throughout the PS experiments, which enhanced the intensity of the R band and promoted its separation from the remaining part of the spectrum (cf. Figure 5a and b). Spectra were first treated with a smoothing procedure according to the Savitzky−Golay algorithm;[25] then, the first derivative of the spectrum was taken with respect to wavelength, and finally, the interception of the spectrum derivative curve with the wavelength abscissa was precisely retrieved according to a linear interpolation procedure. By this three-step spectroscopic procedure, the R-band maximum could be located with a relatively high precision. A typical smoothed derivative curve and the related linear interpolation procedure are shown in Figure 6 for the R band of pure SiO_2 glass (cf. Figure 4) recorded at 8 kV. In the case of C-doped SiO_x, the presence of the Y band, the unknown contribution from contaminating carbon, is a quite disturbing factor when deconvolution is attempted for isolating a given sub-band from the SiO_x spectrum for stress assessment purposes. In addition, the R band is fully embedded in the CL spectrum, and a precise assessment of the R-band-top spectral shift is ill-defined. For this reason, stress-related spectral shifts of the R band of SiO_x were monitored on its low-energy foot at a fixed relative intensity of 0.2. Note that no additional bands are present on this side of the CL spectrum, and this choice should minimize the effect of local intensity fluctuations of the Y band on the observed PS sensitivity of NBOHC.

Figure 7 shows the dependence on stress of the spectral position of the oxygen-excess R band located at around 630 nm when excited at 8 kV. The plot is cumulative for the two materials investigated and for the three types of calibration methods (i.e., four-point bending and indentation crack-tip and print-edge calibrations). Consistency is found between the slopes (i.e., the PS coefficients) retrieved from macroscopic and microscopic calibration methods, demonstrating the validity of the PS assessment in SiO_x glass and of the PRF spatial convolution approach to PS assessments.

D. Application of the PS Technique to Residual Stress Analysis at SiO_x/Si Interface. Figure 8a shows a FEG-SEM micrograph taken at the SiO_2/Si interface of an intermediate unit in a CVD MOS device. Several line scans were collected at different acceleration voltages (6, 8, and 10 kV) along a selected line in the silica area across the silicon interface, as
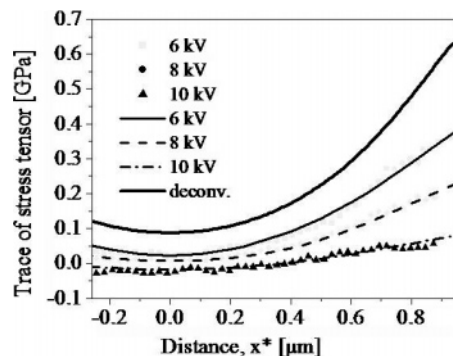
Figure 9. Plots of the CL experimental residual stress and convoluted stress tensor traces, as observed and calculated with scanning at different accelerating voltage values and given as a function of distance x^*.

shown by dots in Figure 8a. Figure 8b and c shows two typical CL spectra, one collected at a location far away from the interface and the other exactly centered at the SiO_x/Si interface (in b and c, respectively; for the locations, cf. larger dots in Figure 8a). Significant morphological changes can be noticed from a comparison between the two CL spectra, which can be summarized as follows: (i) The relative intensity of the B band with respect to that of the R band was found to conspicuously increase when approaching the Si interface, until reaching approximately the same level of the R band in the spectrum recorded at the interface. This strongly suggests that the oxygen defect population changes dramatically in the neighborhood of the SiO_x/Si interface, with a conspicuous increase of ODC toward the interface. (ii) Although no carbon was intentionally added to silica in this sample, the relative intensity of the Y band was more pronounced at the interface, suggesting that C impurities tend to segregate to the SiO_x/Si interface. In the collected series of CL spectra, we monitored the 650 nm oxygen-related silica band with respect to its wavelength shift. Band shifts were then converted into trace values of stress tensor according to the average PS coefficient given in Figure 7. Plots of the stress tensor traces, as observed with scanning at different V values and given as a function of distance x^* (defined in Figure 8a), are shown in Figure 9. Decreasing the accelerating voltage, and thus the CL probe size, the interface stress magnitude at the silica/silicon interface increased. This observation can be interpreted by considering the high stress gradient present in the proximity of the interface and the finite size of the electron probe, which decreases drastically with decreasing acceleration voltage (cf. experimental plot in Figure 1c).

The residual (thermal) stress field due to fully embedded rectangular inclusions has been described by Hu[26] according to the Green's function approach. For brevity sake, we shall not

3934 *J. Phys. Chem. A, Vol. 112, No. 17, 2008*

Leto et al.

repropose in this article a detailed description of the Hu's model but limit our treatment to the salient equations of the model. More details on the stress assessment approach in Si-based devices can be found in a recently published paper on C-doped SiO_x/Si devices.[19] As explained at the outset, the output of a PS assessment is the spectral shift, $\Delta\lambda$, which can be directly related to the trace of the principle stress tensor. Let the trace of the convoluted (thermal) residual stress tensor, $<\overline{\sigma_{ii}^*}>_T(y_0,z_0)$, stored in the neighborhood of the silica/silicon interface, be expressed according to the following integral (cf. our choice of Cartesian coordinates in Figure 8a)

$$<\overline{\sigma_{ii}^*}>_T(y_0,z_0 \approx 0) =$$

$$\frac{\int_0^{+\infty}\int_0^{+\infty} G(y;y_0;z,z_0;V) <\sigma_{ii}^*>_T(y,z)\mathrm{d}y\mathrm{d}z}{\int_0^{+\infty}\int_0^{+\infty} G(y;y_0;z,z_0;V)\mathrm{d}y\mathrm{d}z + \int_{-\infty}^0\int_Z^{+\infty} G(y;y_0;z,z_0;V)\mathrm{d}y\mathrm{d}z} +$$

$$\frac{\int_{-\infty}^0\int_Z^{+\infty} G(y;y_0;z,z_0;V) <\sigma_{ii}^*>_T(y,z)\mathrm{d}y\mathrm{d}z}{\int_0^{+\infty}\int_0^{+\infty} G(y;y_0;z,z_0;V)\mathrm{d}y\mathrm{d}z + \int_{-\infty}^0\int_Z^{+\infty} G(y;y_0;z,z_0;V)\mathrm{d}y\mathrm{d}z} \quad (12)$$

where $<\sigma_{ii}^*>_T(y,z) = \sigma_{xx}(y,z) + \sigma_{zz}(y,z)$ is the trace of the thermal residual stress tensor. In other words, the bias involved with the finite size of the probe can be taken into consideration and corrected by exploiting the knowledge of the PRF of the material. The retrieved convoluted stress traces, $<\overline{\sigma_{ii}^*}>_T(y_0,z_0)$, can be computed according to the knowledge of the PRF, $G(y,z;y_0,z_0 \approx 0;V)$, for silica, which is given in eq 1. It should be noted that, from a mathematical point of view, finding the function $<\overline{\sigma_{ii}^*}>_T(y)$ from the experimental values $<\overline{\sigma_{ii}^*}>_T(y_0,z_0)$ means solving the inverse integral eq 12. A solution can be found only if the character of the $<\overline{\sigma_{ii}^*}>_T(y)$ function is known. According to Hu,[26] the elastic stress field stored in a fully embedded array of parallelepipedic inclusion at the ith inclusion (belonging to a regular array of $2N$ inclusions with infinite length along a Cartesian x-axis but finite width and depth) has been shown in a previously published paper.[19]

In the calculation, the parameter, Δ^{19} was selected to best fit the experimental curve. Both functions $<\overline{\sigma_{ii}^*}>_T(y,z)$ and $<\overline{\sigma_{ii}^*}>_T(y_0,z_0,V)$, corresponding to the spatially deconvoluted stress tensor trace distribution and to the (best-fitting) convoluted stress tensor trace distributions, respectively, are also shown in Figure 9. The former stress distribution corresponds to the real stress distribution in the neighborhood of the SiO_x/Si interface, after correction of the probe bias arising from electron scattering in the material. As can be seen, the tensile stress magnitude at the interface is of a non-negligible magnitude and calls for further improvements in device processing in order to achieve more mechanically and chemically stable interfaces. Through the efforts of many theoretical works in the last three decades, essential understanding has been achieved of the sources and the mechanisms behind these problems, and sound three-dimensional descriptions of stress states have been put forward. This work builds upon the theoretical findings and shows how quantitative experimental stress information can be obtained on a nanometer scale by using the optical activity of oxygen defects in silica glass. This new approach, which we have shown to apply independent of chemical and defect population details in the glass network, may in the near future become instrumental in the optimization of process conditions, materials parameters, and structural geometry of advanced silicon integrated-circuit chips.

4. Conclusions

Experimental measurements of localized stresses around embedded patterns have been obtained by using the PS response of NBOHC ($\equiv$Si$-$O•) present in the silica amorphous network. Specifically, the wavelength shift of the R line, excited by a highly focused electron beam, has allowed achievement of a relatively high spatial resolution in the sub-micrometer scale. Efforts were made in minimizing the effect of the finite size of the electron probe (i.e., due to electron scattering in the material) on the resolution of the stress measurement. In this context, a spatial deconvolution procedure has been proposed, according to which the actual stress distribution could be retrieved from experimental stress data (i.e., convoluted within the electron probe volume), using a Gaussian-like probe response function suitable for silica glass. In addition, it has been shown that the adopted PS approach can be also applied to silica glasses containing carbon dopant/impurity and, more in general, that spectrally/spatially resolved CL spectroscopy can bring a combined piece of information including both chemical and micromechanical aspects of SiO_x/Si interfaces.

References and Notes

(1) Morrison, C. A.; Leavitt, R. P. In *Handbook on the Physics and Chemistry of Rare Earths*; Gschneider, K. A., Eyring, L., Eds.: North Holland: Amsterdam, The Netherlands, 1982; Vol. 9, Chapter 46.

(2) Weber, M. J. In *Laser Spectroscopy of Solids*; Yen, W. M., Selzer, P. M., Eds.; Springer: Berlin, Germany, 1981; p 189.

(3) Weber, M. J. *Ceram. Bull.* **1985**, *64*, 1439.

(4) Blasse, G. *Chem. Phys. Lett.* **1973**, *20*, 573.

(5) Hegarty, J.; Brundage, R.; Yen, W. M. *Appl. Opt.* **1980**, *19*, 1889.

(6) Skuja, L. *J. Non-Cryst. Solids* **1998**, *239*, 16.

(7) Pezzotti, G. *Microsc. Anal.* **2003**, *5*, 5.

(8) Pezzotti, G.; Leto, A.; Tanaka, K.; Sbaizero, O. *J. Phys.: Condens. Matter* **2003**, *15*, 7687.

(9) Leto, A.; Pezzotti, G. *J. Phys.: Condens. Matter* **2004**, *16*, 4907.

(10) Pezzotti, G. *J. Raman Spectrosc.* **1999**, *30*, 867.

(11) De Portu, G.; Micele, L.; Sekiguchi, Y.; Pezzotti, G. *Acta Mater.* **2005**, *53*, 1511.

(12) Donolato, C. *Phys. Status Solidi A* **1981**, *65*, 649.

(13) Porporati, A. A.; Hosokawa, K.; Zhu, W.; Pezzotti, G. *J. Appl. Phys.* **2006**, 100, 093508.

(14) Porporati, A. A.; Tanaka, Y.; Matsutani, A.; K.; Zhu, W.; Pezzotti, G. *J. Appl. Phys.* **2006**, 100, 083515.

(15) Kanaya, K.; Okayama, S. *J. Phys. D.: Appl. Phys.* **1972**, *5*, 43.

(16) Grabner, L. *J. Appl. Phys.* **1978**, *49*, 582.

(17) Fett, T. Forschungszentrum Karlsruhe Report No. FZKA **2002**, 6757.

(18) Yoffe, E. H. *Philos. Mag. A* **1982**, *46*, 617.

(19) Leto A.; Porporati A. A.; Zhu W.; Green M.; Pezzotti G. *J. Appl. Phys.* **2007**, *101*, 093514.

(20) Zhu, W.; Porporati, A. A.; Matsutani, A.; Lama, N.; Pezzotti, G. *J. Appl. Phys.* **2007**, *101*, 103531.

(21) *MATHEMATICA 5.0*; Wolfram Research, Inc.: Champaign, IL, 2003.

(22) Fitting, H.-J.; Glaefeke, H.; Wild, W. *Phys. Status Solidi A* **1977**, *43*, 185.

(23) Skuja, L. *J. Non-Cryst. Solids* **1994**, *179*, 51.

(24) Koyama, H. *J. Appl. Phys.* **1980**, *51*, 2228.

(25) Press, W. H.; Teukolsky, S. A.; Vettering, W. T.; Flannery, B. P. *Numerical Recipes in C*; Cambridge University Press: Cambridge, England, 1992.

(26) Hu, S. M. *Appl. Phys. Lett.* **1978**, *32*, 5−7.